Pseudorange measurement and Sun phase angle estimation using CNN-based Image Processing algorithm for Hera mission

Aurelio Kaluthantrige
University of Strathclyde, mewantha.kaluthantrige-don@strath.ac.uk
Jinglang Feng
University of Strathclyde, jinglang.feng@strath.ac.uk

Jesús Gil-Fernández
ESA/ESTEC, Jesus.Gil.Fernandez@esa.int

ABSTRACT

Hera is the European Space Agency (ESA)'s Space Situational Awareness contribution to the international collaboration Asteroid Impact Deflection Assessment, the first planetary defense mission. The Early Characterization Phase (ECP) of the Hera mission is a proximity operation that has the objective of conducting physical and dynamical characterizations of binary asteroid system (65803) Didymos. In this phase, an Image Processing (IP) algorithm is designed to estimate the position of the Center of Mass (COM) of the primary to enable Line of Sight navigation. To measure the range with Didymos, Hera uses the Planet ALTimeter (PALT), a lidar experiment that is not operating during the ECP as it requires closer distances with Didymos. However, standard IP algorithms need to introduce correction terms depending on the Sun phase angle (Sun-asteroid-spacecraft) to increase the accuracy of their estimation. Within this context, this paper develops a methodology to measure the pseudorange with the primary and to estimate the Sun phase angle by exploiting a Convolutional Neural Networks (CNN)-based IP algorithm. The training, validation and testing datasets are generated with the software Planet and Asteroid Natural scene Generation Utility (PANGU). For the first aim, the proposed methodology regresses a set of keypoints on the visible border of Didymos and evaluates its apparent radius, which is used to measure the pseudorange with the spacecraft. For the second aim, the methodology measures the Sun phase angle using the pixel position of the subsolar point of the primary. The High-Resolution Network (HRNet) is used as CNN architecture as it represents the state-of-the-art technology in keypoint detection. The HRNet-based IP algorithm measures the pseudorange and estimates the position of the subsolar point with high accuracy. The Sun phase angle estimation is accurate with limited dependence on the shape of the asteroid.

1. INTRODUCTION

The Asteroid Impact Deflection Assessment (AIDA) is an international collaboration between the National Aeronautics and Space Administration (NASA) and the European Space Agency (ESA), with the primary objective of investigating a binary asteroid system and to demonstrate its deflection by kinetic impact. The NASA contribution to this mission is the Double Asteroid Redirection Test (DART), a kinetic impactor launched on the 24th of November 2021 that will perform the deflection in September 2022 [9]. ESA's segment of the AIDA mission is represented by Hera, whose objectives are to research on the properties of the binary asteroid system, to observe the results of DART's impact and to assess the feasibility of the deflection technique [8]. Hera falls under ESA's Space Situational Awareness (SSA) initiative, which enables ESA to detect, predict and assess the risk of Near Earth Objects. The target of this mission is the near-Earth asteroid (65803) Didymos and its moon Dimorphos. Table 1 illustrates relevant properties of Didymos and Dimorphos. The spin axis of both bodies is orthogonal to the binary's orbital plane. Dimorphos is tidally locked with Didymos, i.e. its rotation period is equal to its revolution period around the primary [6].
The proximity operations of Hera consist of different phases that depend on the mission objectives. The focus of this work is the Early Characterization Phase (ECP), with the spacecraft at a distance of around 30 *km* from the target with the objective of conducting physical and dynamical characterizations of Didymos [5].

Table 1: Didymos' system properties [6]

Parameter	**Didymos**	**Dimorphos**
Gravitational parameter $[km^3/s^2]$	$3.5225 \cdot 10^{-8}$	$2 \cdot 10^{-10}$
Diameter $[m]$	780	164
Rotation period $[hours]$	2.26	11.92
Obliquity of the binary orbit with Ecliptic plane	169.2°	169.2°

Observing a binary asteroid system from such a short distance is unprecedented. A vision based Guidance, Navigation and Control (GNC) system is designed to improve the mission autonomy. This system comprises an on-board camera taking images of the asteroid, an Image Processing (IP) algorithm that extracts information from these images, and a navigation filter that is able to process the visual data to estimate the spacecraft position, velocity and attitude with respect to the binary system. The camera used for the vision based navigation system is the Asteroid Framing Camera (AFC). For the ECP, the navigation strategy is centroid-based, meaning that the IP algorithm is designed to extract the Center of Mass (COM) of the primary body, thus estimating the Line Of Sight of the spacecraft, with the purpose of enabling autonomous attitude navigation [11]. Nevertheless, standard IP algorithms' performances are highly depending on the intrinsic properties of the captured images. Factors such as the Signal-to-Noise ratio, illumination conditions, the presence of other bodies in the image and the irregular shape of the asteroid can affect the accuracy of the extracted visual information. To reduce the error caused by the illumination conditions, standard IP algorithms introduce correction terms that depend on the Sun phase angle and improve the accuracy of the estimation of the position of the COM.

To estimate the relative position of the spacecraft, range measurements with the asteroid are required. The on-board instrument to measure the range with Didymos is the Planet ALTimeter (PALT), a lidar experiment that determines the distance to the asteroids with an accuracy of 0.5 m by measuring the time of flight of a laser beam at 1.5 μm of wavelength. PALT is operational at a distance ranging from 500 m to 14 km, hence it cannot be used to determine the range with Didymos during the ECP [1].

This work addresses the challenges related to the irregular shape of the asteroid and the presence of the secondary body in the images. We develop a Convolutional Neural Network (CNN)-based IP algorithm that estimates the range with Didymos and the Sun phase angle limiting the errors introduced by these two factors. Since it is not a direct measurement but it is derived from the images, the estimated range is a pseudorange measurement. With these two measurements the navigation filter is able to estimate the relative position of the spacecraft with respect to Didymos, increasing the robustness of the navigation strategy and of the proximity operations.

Recent years have seen an increase of the implementation of CNNs in space image processing. One of the main advantages of CNNs with respect to standard IP algorithms is the robustness over disturbances and adverse characteristics of the images. Most of the CNNs process the input image with a network typically consisting of a series of high-to-low resolution subnetworks. This process reduces the input's resolution, which is then recovered through a low-to-high process. With this procedure, extracted visual data have low spatial precision and accuracy that are important aspects for an autonomous attitude navigation system. Therefore, this works adopts the High-Resolution Network (HRNet) architecture to maintain a high-resolution representation through the whole network [16]. This process leads to a keypoints regression with superior spatial precision and higher accuracy. The HRNet is used in this work to estimate in the images the positions of a set of keypoints which are then processed using the pinhole camera model to measure the pseudorange and the Sun phase angle. One unique contribution of our work is the regression of the subsolar (SS) point on the surface of Didymos, which is leveraged with a novel methodology to estimate the Sun phase angle.

This paper is structured as follows. Section 2 reviews the state of the art of methodologies applied for range and phase angle estimation from images of asteroids. Then, Section 3 describes the framework of our methodology. Section 4 performs the numerical simulations and analyze the results obtained. Finally Section 5 concludes this research and recommends future research directions.

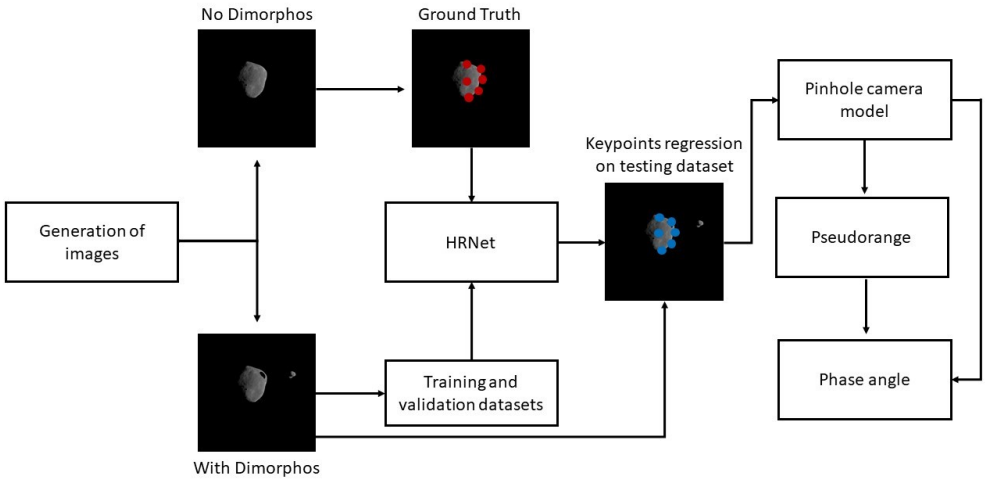

Fig. 1: Overall pipeline of HRNet-based IP algorithm for pseudorange and phase angle estimation

2. RELATED METHODS

To the author's knowledge, the methodologies to estimate the range and the Sun phase angle from images are limited, as these parameters are usually obtained from other sensors. In this Section, current IP algorithms used for this purpose are reviewed.

2.1 Pseudorange

Methods that rely on the calculation of the apparent radius have been proposed [12]. By comparing the radius of the asteroid with the major length (δ) of the projection of the asteroid on the image plane, the range is calculated. Nevertheless, the estimated range is noisy and not accurate, as the irregular shape of the asteroid provides different values of δ. In this work, this algorithm is expanded to meet the accuracy requirements for the navigation strategy of Hera [4]. The error introduced by the shape of Didymos is reduced by calculating multiple values of δ for each image.

2.2 Phase angle

[13] compared different methodologies to measure the Sun phase angle from a database of images of Didymos generated with the 3D computer graphics software Blender. The first method relies on a correlation that has been found between the eccentricity e of the asteroid and the phase angle γ. This correlation has been modelled using a second-order polynomial as in Eq. 1.

$$\gamma(x) = p_2 e^2 + p_1 e + p_0 \tag{1}$$

The coefficients of the polynomial have been calculated by fitting the data in the least-square sense, and they are $p_0 = 10.31$, $p_1 = 12.42$ and $p_2 = 92.15$. The estimation of the Sun phase angle is accurate for larger phase angle values. The second method involved the utilization of neural networks and CNNs to spot relationships between different geometrical features of the asteroid, such as the eccentricity, orientation and circularity. It has been found that the CNNs outperform all the other methods with their capability of extracting spatial information from images. In this work the CNNs are used to estimate the position of the SS point, which is used to estimate the Sun phase angle.

3. METHODOLOGY

In this Section, the methodology of this research is described. Fig. 1 shows the main steps of the undertaken pipeline. With the ECP reference trajectory and Planet and Asteroid Natural scene Generation Utility (PANGU), two sets of images are generated, one without the presence of Dimorphos and one with both bodies. The former set is processed to retrieve the Ground Truth (GT) keypoints which are used to supervise the training and validation of the HRNet. The GT keypoints are 26 points selected from the projected surface of the primary on the image plane which include: the

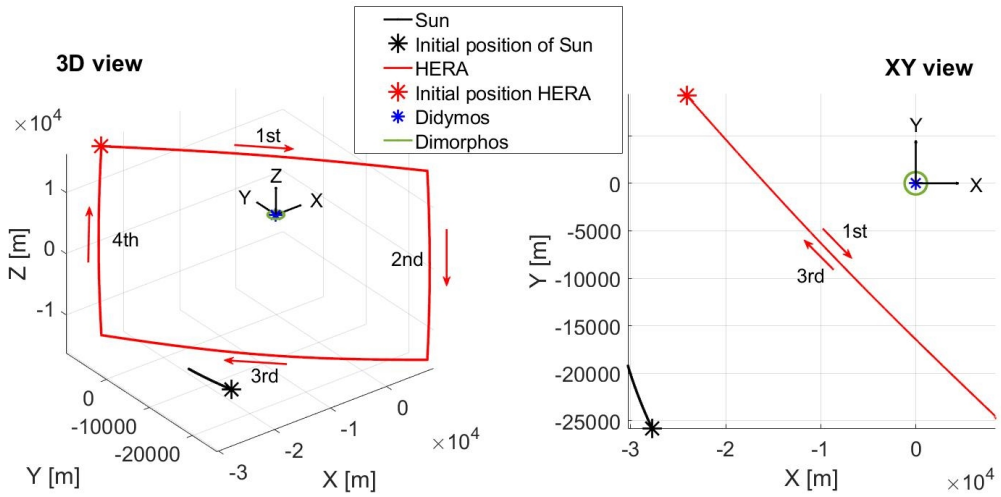

Fig. 2: ECP trajectory

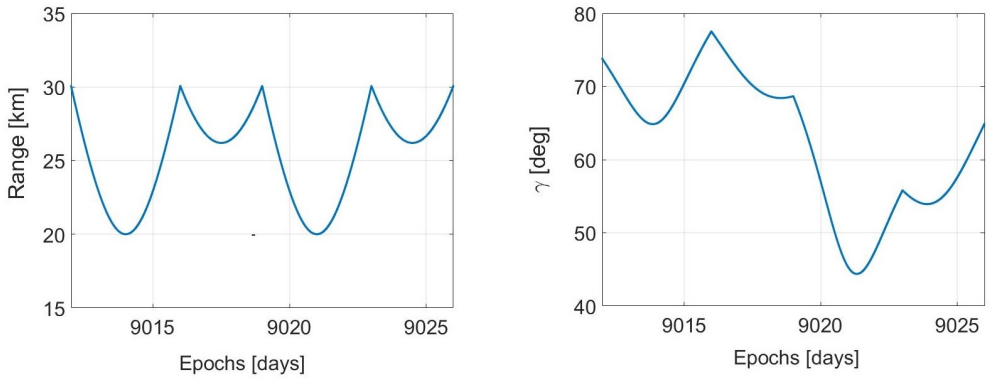

Fig. 3: Range and phase angle of the ECP trajectory

COM, 24 points on the visible border and the SS point. The second set of images is used for the training, validation and testing of the HRNet.

The trained HRNet is applied to estimate the position of the keypoints of the testing dataset with both bodies. Finally, the pinhole camera model is used with the estimated keypoints to measure the pseudorange and to estimate the Sun phase angle. Details of the main steps are described in the rest of this section.

3.1 Reference trajectory

The adopted reference frame is the Target Body Equatorial Inertial (TBEqI), which has the origin located on Didymos, the X-axis pointing towards the vernal equinox, and the XY plane coplanar to the equatorial plane of Didymos. The relative motion of the Sun around Didymos is retrograde as the binary system's orbit obliquity with respect to the Ecliptic plane is higher than 90°, as shown in Table 1.

The ECP trajectory data is provided by ESA. Fig. 2 represents the trajectory of the spacecraft, together with the position of the Sun (scaled down in the illustration) and the orbit of the secondary. The position of the Sun is calculated using the Jet Propulsion Laboratory Small Body Database [10]. The trajectory consists of 4 hyperbolic arcs, with an initial epoch of $t_{in} = 9012$ days and a final epoch of $t_{fin} = 9026$ days, calculated in the Modified Julian Date 2000. The only forces considered for each arc are the point mass gravitational attractions of both the primary and the secondary. Orbital manoeuvres are performed at the joint of two arcs. The duration of the 1^{st} and 3^{rd} arcs is 4 days while the duration of the 2^{nd} and 4^{th} arcs is 3 days. The range with respect to the primary varies between a minimum of 20 km and a maximum of 30 km as shown in Fig. 3.

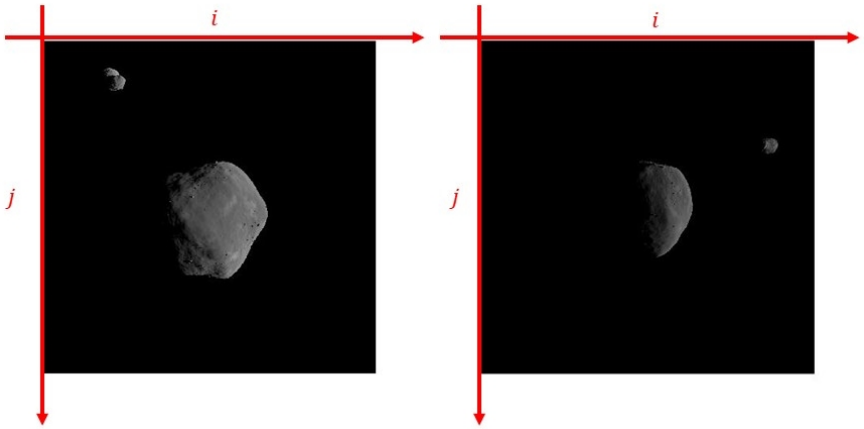

Fig. 4: PANGU viewer with two sample images captured at different points of the ECP trajectory

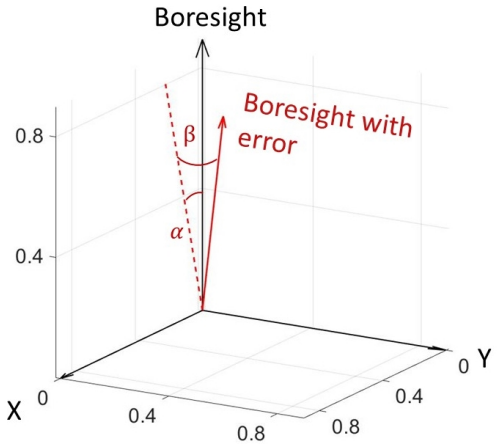

Fig. 5: Camera pointing with error

It can be seen from Fig. 2 that the ECP trajectory is interposed between the Sun and Didymos, in order to provide the AFC camera with bright images for the centroiding navigation [5]. Fig. 3 shows that the phase angle γ for the ECP trajectory is lower than 90°, meaning that Hera is always seeing the day side of the asteroid.

3.2 Generation of images

The software PANGU is used to generate the database of images for this work. PANGU is a simulation tool that models planet and asteroids surfaces and provides a high degree of realism in the visualization of images while operating at near real-time speeds. The software has been developed by the STAR-Dundee engineering company [2]. The models of Didymos, Dimorphos and the camera are provided by GMV Aerospace and Defence, in charge of the GNC system of the Hera mission. Didymos' shape is near-spherical, and it is a spinning top with an elevated ridge along the equator. The shape of Dimorphos is not well known and it is approximated by scaling down the shape model of Itokawa that was the target asteroid of the Hayabusa mission.

The software generates the images detected by the camera and shows them on the PANGU viewer, a plane with the size of the image (shown in Table 2) and the origin of the coordinated frame set to the top left corner. The horizontal and the vertical axes of the plane are referred to as i-direction and j-direction respectively. In order to visualize the binary system of asteroids on PANGU, the flight file system is operated. These files control the PANGU viewer and generate images taken at selected points of the reference trajectory in the TBEqI reference system, considering the position of the Sun (range, Azimuth and Elevation) and the positions and the orientations (quaternions) of both the

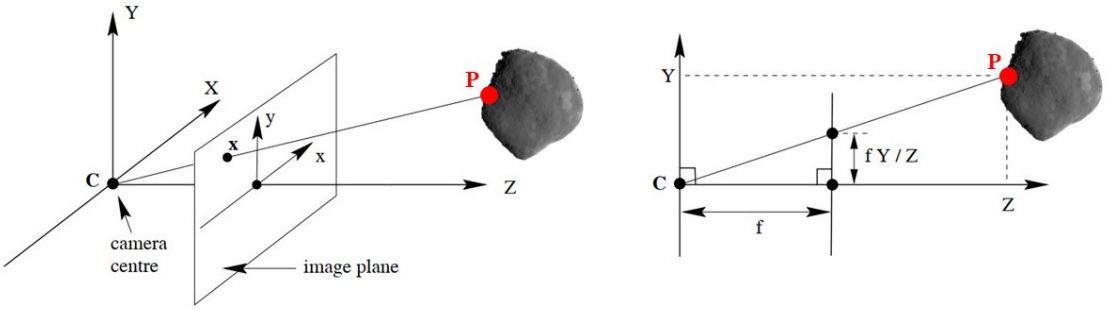

Fig. 6: Pinhole camera model geometry [7]

binary asteroid system and of the AFC camera (joined with the spacecraft) [2]. During asteroid imaging, the AFC has its boresight pointing towards the primary and the vertical axis of the camera is perpendicular to the direction of the Sun with respect to Hera [5]. PANGU adopts the boresight, the vertical and the horizontal axis of the camera respectively as the Z- the Y- and the X-axis of the camera reference frame [2]. Therefore, the position vector of the Sun with respect to Hera lies on the XZ plane of the camera frame. As a result, the images generated on the PANGU viewer always represent the binary system illuminated from the right side. Fig. 4 shows two sample images generated at different points of the ECP trajectories, together with the *i*- and the *j*-directions of the PANGU viewer.

When the camera is pointing perfectly towards the primary, the latter is displayed in the middle of the PANGU viewer. With these conditions, the Geometrical Center (GC) of the PANGU model of the primary, that is the arithmetic mean position of all the points belonging to the body, is located at the central pixel with the coordinates $(i, j) = (512, 512)$ *pixels* in the PANGU viewer. Because of its near-spherical shape, the COM of the primary almost coincides with its GC. Since the images used in this work are all generated with PANGU, it is assumed that the GC of Didymos is its centroid. If the camera's boresight is always pointing perfectly towards the GC of the asteroid, its position on the PANGU viewer will always be $(i, j) = (512, 512)$ *pixels* for each image. Training the CNN algorithm with a set of images with these characteristics will result in an issue of lacking label variability. To overcome this issue a pointing error represented by spherical coordinates and defined by two angles α and β is introduced at each point of the trajectory in the boresight direction of the camera reference system, as shown in Fig. 5, so that the generated images are shifted from the central position of the PANGU viewer.

In order to make sure that the asteroid is within the Field of View (FOV) of the AFC camera, random values within an interval of $[-1, 1]^\circ$ are considered for both α and β. With these values, the primary location is shifted around the viewer. By calculating the shift in pixels of the primary from its central position, the pixel coordinates of the COM of the primary is calculated for each value of α and β.

3.3 Pinhole camera model

The pinhole camera model is implemented in PANGU using the properties of the AFC camera, shown in Table 2 [3, 14]. In the pinhole camera model, also called perspective camera model, the camera aperture is considered as a

Table 2: AFC properties [3, 14]

FOV	Focal Length: f	Aperture	Image size	Pixel Size: ν
5.5°	10.6 *cm*	2.5 *cm*	1024×1024 *pixels*	14 μm

point rather than a lens. Therefore, this model is used to achieve a first-order approximation of the relationship between the coordinates of a point in the 3D space and its projection onto the 2D image plane of the camera [15]. Fig. 6 shows the geometry of a pinhole camera model. In this model the centre of projection **C** is the origin of the camera reference frame and the image plane is located at the focal length $f = 10.6$ *cm* (Table 2). It can be seen from Fig. 6, that a point in space **P** with coordinates (X, Y, Z) is mapped to a point on the image plane with the coordinates $(\frac{fX}{Z}, \frac{fY}{Z}, Z)$ [14]. The units conversion from meters to pixels for an object of length l on the image plane is given by $n \cdot \nu$ *pixels*, where n is the number of pixels representing the object and ν is the pixel size (Table 2). Therefore, an object of length L in

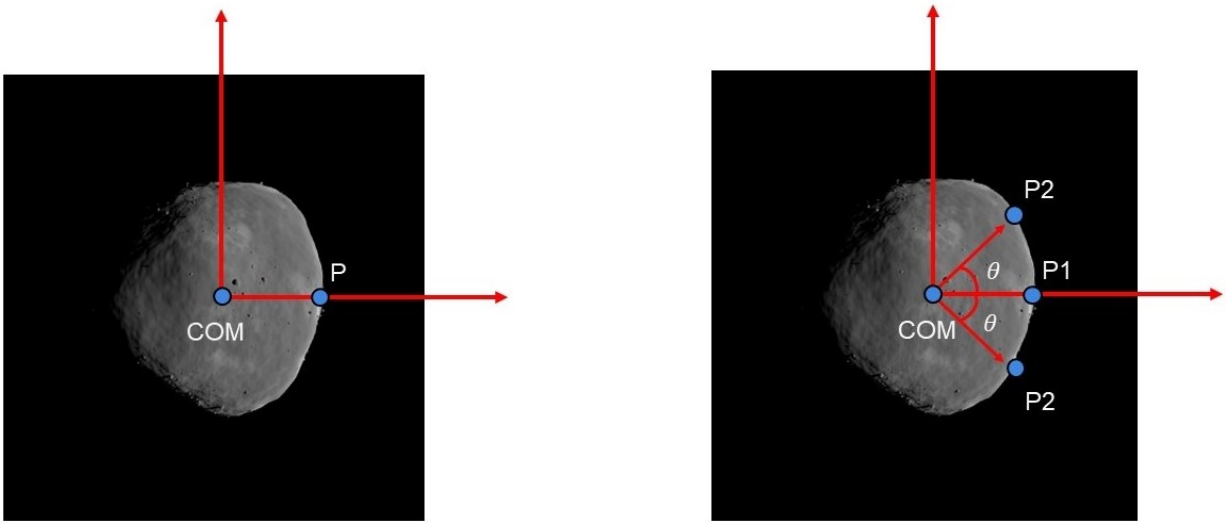

(a) Two points (b) Multiple points

Fig. 7: Keypoints selected from the visible border of the asteroid

meters on a plane of the 3D space at distance Z from the camera and parallel to the image plane is projected onto the latter with the dimensions in pixels defined by Eq. 2.

$$n \cdot \nu = \frac{f \cdot L}{Z} \tag{2}$$

3.4 Keypoints for the pseudorange

In order to apply the pinhole camera model to measure the pseudorange of the spacecraft with respect to Didymos, the shape of Didymos is approximated as a sphere of radius $R = 390\ m$ (Table 1). Given that on the image plane the length of the asteroid radius has a value of $n_R\ pixels$, Z can be solved from Eq. 2, which is the distance from the centre of projection **C** and the COM of Didymos, i.e. the range. Therefore, once n_R of an image captured by the camera is obtained, the range can be calculated with Eq. 3.

$$Pseudorange = \frac{f \cdot R}{n_R \cdot \nu} \tag{3}$$

Fig. 7a shows how n_R is calculated for a generic synthetic image of the asteroid, which is measured by the number of pixels from the COM, determined in Section 3.2, to the point P on the asteroid's border along the i-direction. Dimorphos is hidden from the images as its presence in front of Didymos or near its border would disturb the evaluation of n_R.

Nevertheless, this calculation of n_R is highly dependant on the relative attitude of Didymos with respect to the spacecraft because of the asteroid's irregular shape. To reduce the error introduced by the irregularity of the shape, multiple points P_i on the border within an arc of angular aperture 2θ are considered, as shown in Fig. 7b. The distance n_R^i is evaluated for each point P_i and the average value $\bar{n}_R$ is calculated and used in Eq. 3 to measure the pseudorange. To find the optimal values for θ and for the number of points P_i that minimize the estimation error, the following steps are taken:

1. Given an image of the asteroid, an arc of angular aperture 2θ with $\theta \in [0, 110]^\circ$ is considered; the maximum value of θ is determined considering that the asteroid is illuminated from the right side of the image plane, as explained in Section 3.2.
2. For each arc, a number of points P_i at an equal angular distance from each other are taken on the asteroid's border; an upper limit of 50 points is selected considering the computational cost of the keypoints regression by the HRNet;

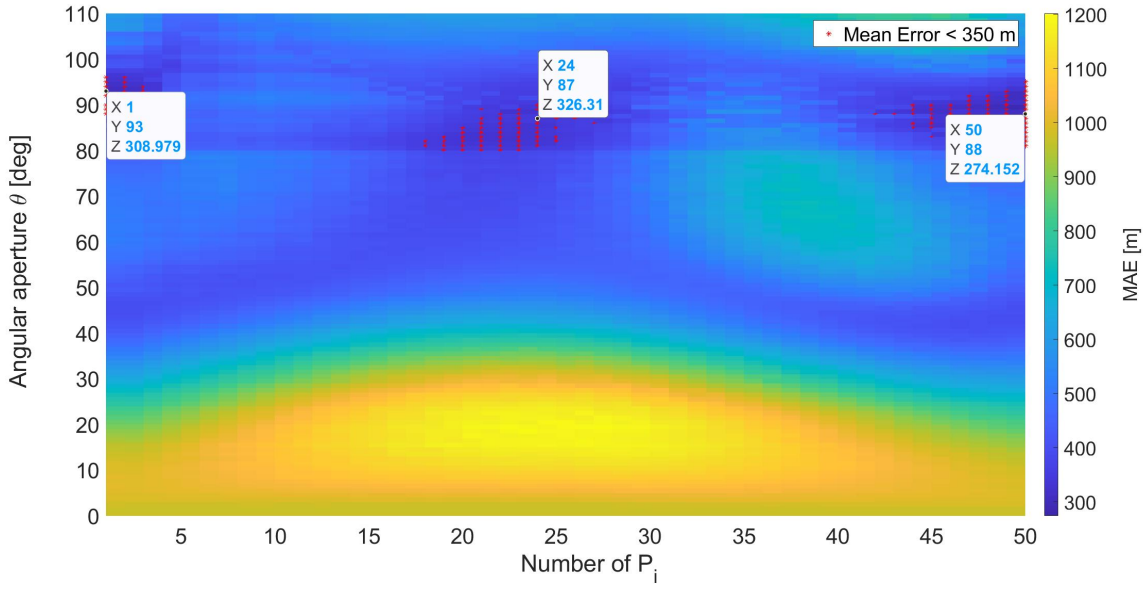

Fig. 8: Optimization of number of keypoints for pseudorange measurement

3. For each point P_i, n_R^i and the average $\bar{n}_R$ are calculated, and the pseudorange with the asteroid is evaluated with Eq. 3.

4. Finally, the pseudorange is compared with the GT range ($Range_{GT}$, obtained from the reference trajectory shown in Section 3.1) for each image and the Mean Absolute Error (MAE) is determined with Eq. 4.

$$MAE = |Pseudorange - Range_{GT}| \tag{4}$$

Following this procedure, Fig. 8 is obtained with the y-axis representing the angle $\theta \in [0,110]^\circ$ and the x-axis representing the number of points $P_i \in [1,50]$. It can be seen illustrated by the red dots that the MAE has its local minima ($MAE < 350\ m$) in three different regions. The minima have a similar value of θ around 90°, and different values of number of points P_i. Hence, considering the whole illuminated side of Didymos instead of only one point on the i-direction justifies the approximation of the shape of the asteroid with a sphere and reduces the error in the pseudorange measurement.

Relying on one singular point, as in the left region of Fig. 8, poses a major risk of failure in the case that the HRNet is not capable of regressing that point accurately. On the other hand, the error obtained with 50 points is not low enough to justify the regression of such a high number of keypoints. Therefore, in this study we select 24 points P_i on the border within an arc of aperture 2θ with $\theta = 87^\circ$.

3.5 Keypoints for the phase angle estimation

The phase angle estimation relies on the SS point of Didymos, as shown in Fig. 9. Given an image captured by the camera, the COM and the SS projections are detected on the image plane. Dimorphos is hidden from the images as it can cause disturbance in the estimation of the position of the SS. The distance in pixels between these two points, defined here as n_P, together with the average radius of the asteroid $\bar{n}_R$, are then used to calculate with Eq. 5 the phase angle γ, as shown in Fig. 9a. Eq. 5 adopts twice the approximation of the shape of the asteroid as a sphere: one for using $\bar{n}_R$ and one for using the inverse of the sine function.

$$\gamma = \arcsin\left(\frac{n_p}{\bar{n}_R}\right) \tag{5}$$

(a) Planar view (b) Image plane view

Fig. 9: Illustration of subsolar point for Sun phase angle estimation

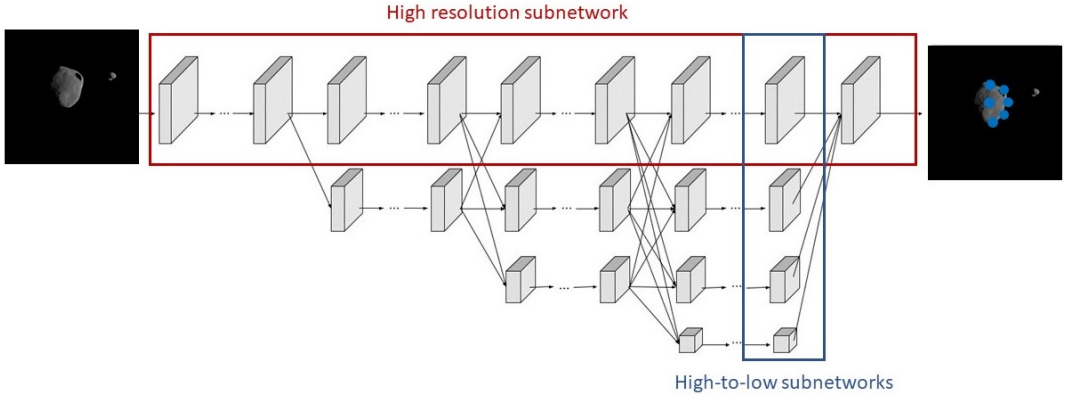

Fig. 10: HRNet architecture

3.6 HRNet

The HRNet architecture is shown in Fig. 10. The network maintains the high resolution representations of the input images by connecting multiple subnetworks in parallel. The first stage is a high-resolution subnetwork. New stages are formed from the gradual introduction of high-to-low subnetworks. To maintain the high-resolution representation, repeated multiscale fusions are performed using low-resolution representation of the same depth and similar level. The last high-resolution representation is then used for the regression of the selected visual data [16].

The keypoints to regress for each image are 26 points on the surface of Didymos, which are the COM, 24 points on the visible border and the SS. Each input image of the HRNet is coupled with the 26 corresponding keypoints that are used to supervise the training to regress the keypoints locations on the testing dataset. In this work, the pose-hrnet-w32 is used, where 32 represent the widths of the high-resolution subnetwork in the last three stages. During training, the validation dataset is used beside the training one to compute the validation losses and avoid overfitting. The Adam optimizer is used with a cosine decaying learning rate with initial value of 10^{-3} and decaying factor of 0.1. The total parameters involved in the training process are $28,536,410$.

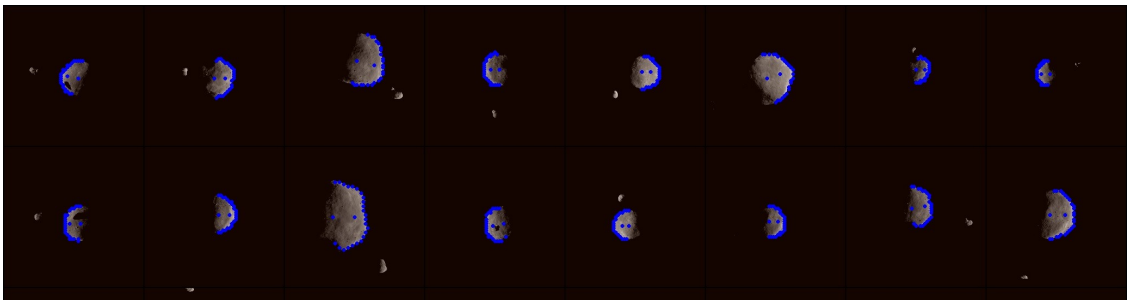

Fig. 11: Sample keypoint detection results during training

The input dataset consists of 12104 (61.53%) images for training, 1513 (7.68%) for validation and 6052 (30.76%) for testing that are obtained by sampling the ECP trajectory respectively every 100, 800 and 200 seconds. Each image show both bodies, so that the HRNet is trained to regress the location of the keypoints despite the disturbance introduced by the presence of Dimorphos. The network is trained for 210 epochs. Fig. 11 shows a mosaic of keypoints detection results on a subset of the training dataset.

4. RESULTS

In this section, the results of the HRNet-based IP algorithm for the measurement of the pseudorange and the estimation of the Sun phase angle are presented. Firstly, the accuracy of the HRNet on the estimation of the positions of the 26 keypoints is analyzed with the metric defined as follows:

$$RMSE_m = \sqrt{\frac{\sum_{n=1}^{N}(P_{mn}^{GT} - P_{mn}^{pred})^2}{N}} \tag{6}$$

where P_{mn} represents the m-th 26 keypoint; the index n refers to the n-th image of the $N = 6052$ images of the testing dataset; $RMSE_m$ is the Root Mean Squared Error (RMSE) between the GT position of the m-th keypoint P_{mn}^{GT} and the estimation P_{mn}^{pred} made by the HRNet. Eq. 6 is applied to all the 26 keypoints. To determine the accuracy of the keypoint regression, the *RMSE* value obtained by the Maximum Correlation with a Lambertian Sphere (MCLS) IP algorithm developed by GMV Aerospace and Defence to estimate the position of the centroid of Didymos during the ECP of the Hera mission is given as a reference: $RMSE_{GMV} = 7.746$ *pixels*. This result is obtained by applying the algorithm over a set of 243 images generated during the ECP.

The accuracy of the results of the pseudorange and the phase angle is assessed through the determination of the error between the GT values and their estimations. The distribution of the error is also analyzed for both parameters, since the optimality of navigation filters assumes the errors having a Gaussian distribution.

4.1 Accuracy of keypoints regression

Fig. 12 is a bar chart of the *RMSE* values obtained for the 26 keypoints regressed by the HRNet. The first and the last bars represent the *RMSE* respectively for the COM and for the SS position estimations. The other 24 points are the ones defined in Section 3.4 on the border of the asteroid. It can be seen that the worst performance of the HRNet is reached for the first point ($\theta = 87°$) of the border of the asteroid and the best performance for the SS point, with values of the *RMSE* equal to 13.161 *pixels* and 1.973 *pixels* respectively.

The difference on the estimation accuracy for each point is depending on the different lighting conditions and on the shape of the asteroid. Nevertheless, the *RMSE* values are very close to the ones obtained by the MCLS IP algorithm. Therefore, the HRNet is able to estimate the position of the GT keypoints with high accuracy independently from the presence of Dimorphos and the irregular shape of the asteroid. Fig. 13 shows 2 images generated by PANGU during the first and the third arc, together with the keypoints estimated by the HRNet.

4.2 Pseudorange measurement

Fig. 14 shows the results obtained for the pseudorange estimation with the HRNet-based IP algorithm. The plot above shows that the estimation is similar to the ground truth illustrated in Fig. 3 in Section 3.1. The plot below in Fig. 14

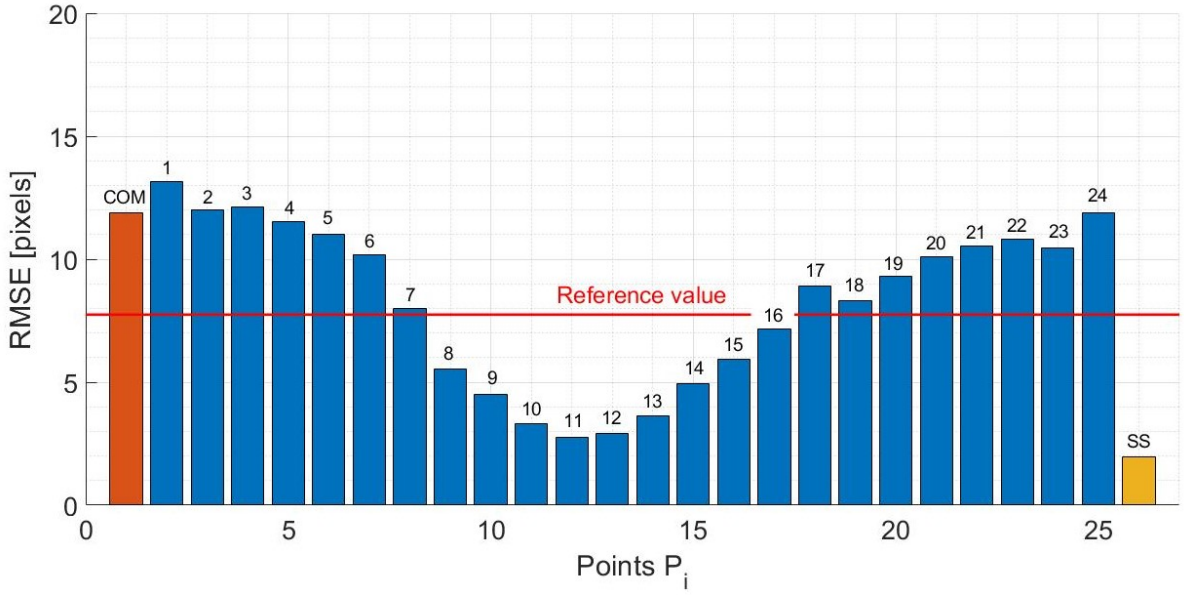

Fig. 12: Accuracy of the keypoints regression

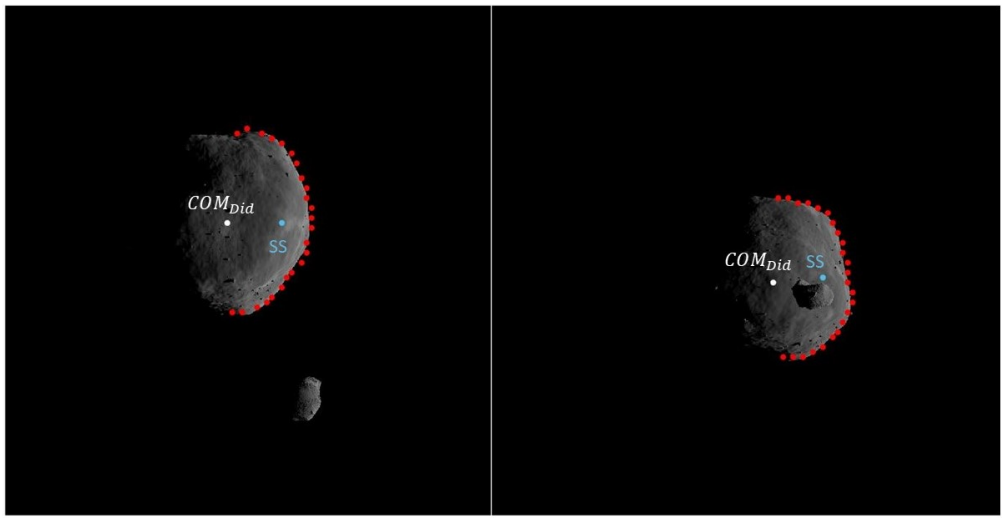

Fig. 13: Keypoints regression results for two images of the 1st and the 3rd arc

shows that the absolute percent error is lower than 10% and it oscillates around a mean value of 2.1385%. It can be seen that when the range reaches its local minima in the 1^{st} and 3^{rd} arcs, the absolute percent error is higher, due to the fact that the images of the asteroid are appearing larger in the image plane. As a consequence, the non-spherical shape becomes more predominant and the approximation as a sphere is less accurate. In particular, the error near the local minima of the range in the third arc is larger because the phase angle is the lowest (Fig. 3) hence the asteroid is brighter and its shape is more visible.

Fig. 15 represents the distribution of the percent error of the pseudorange estimation, which is similar to a white noise with the mean value of $\mu = 0.1298\%$ near 0. It means that the designed algorithm does not suffer from any systematic errors. The value of the error that occurs the most, which is represented by the highest peak of the histogram, is 0.4695%. The standard deviation of the error is $\sigma = 2.6888\%$ which means that 68.27% of the pseudorange measurements have a percent error ranging between $-2.559\%$and 2.8186% with respect to the ground truth. The distribution of the error is symmetrical ($skewness = 0.0176$) and light-tailed ($kurtosis = 3.0067$) which means that the

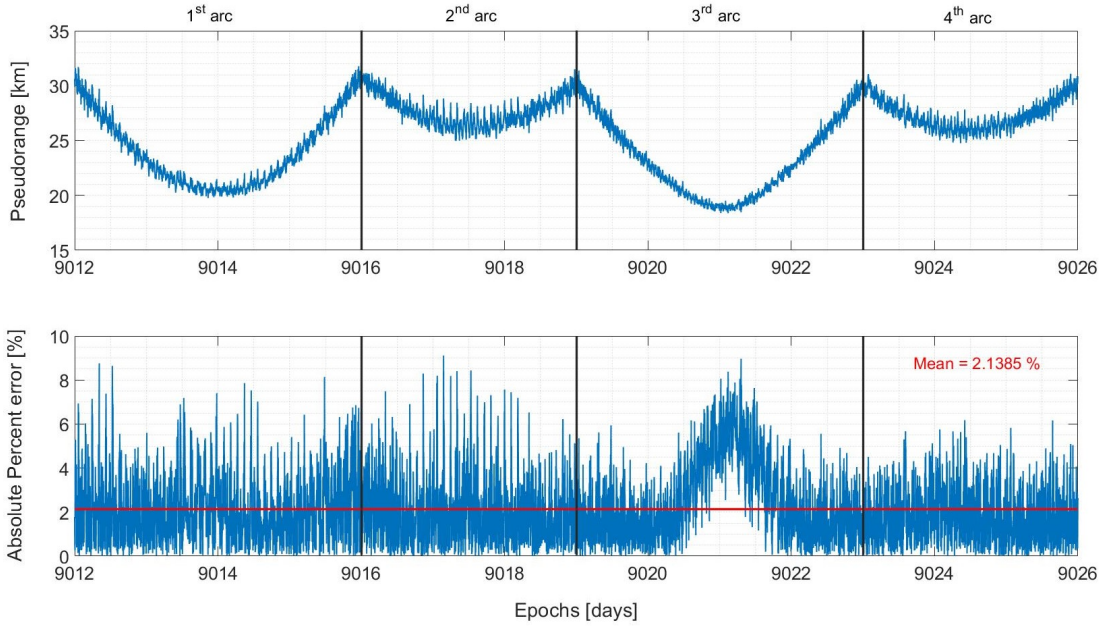

Fig. 14: Pseudorange estimation

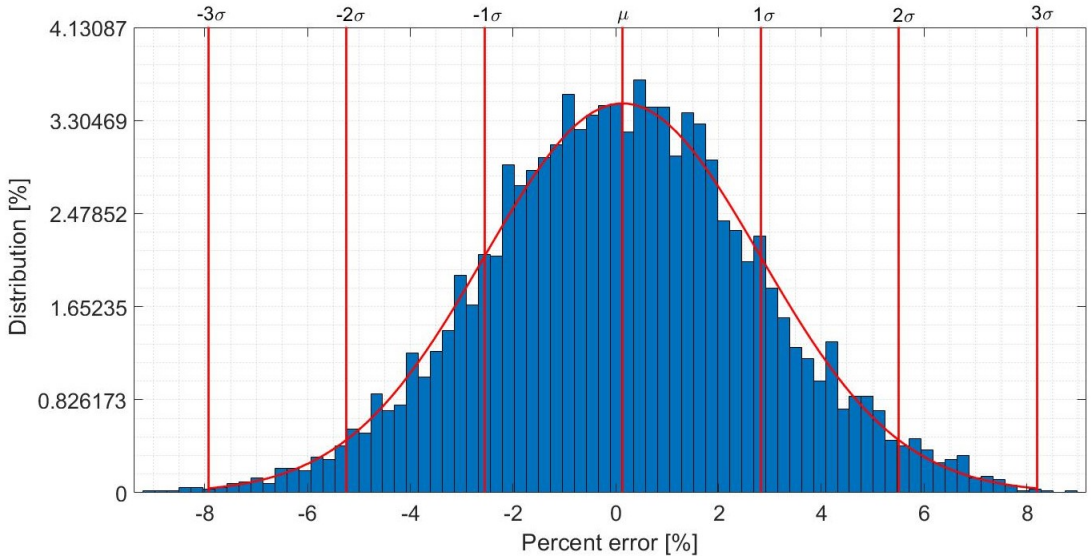

Fig. 15: Pseudorange percent error distribution

percent error distribution is similar to a Gaussian distribution.

4.3 Phase angle estimation

Fig. 16 shows the phase angle estimation obtained by the HRNet-based IP algorihtm. It can be seen that the absolute error is moderate and reaches peaks of 20°, although the SS position on the images is estimated with high accuracy, as shown in Fig. 12. The error is higher because the approximation of the shape of the asteroid used for the estimation of the phase angle is introduced twice in Eq. 5. Nevertheless, the mean error is small (6°) and the estimated phase angle is similar to the GT value shown in Fig. 3.

Fig. 17 illustrates the distribution of the error of the phase angle estimation. Contrarily to the pseudorange estimation, here the white noise approximation is not accurate considering that the mean value of the error is high ($\mu = 5.976°$).

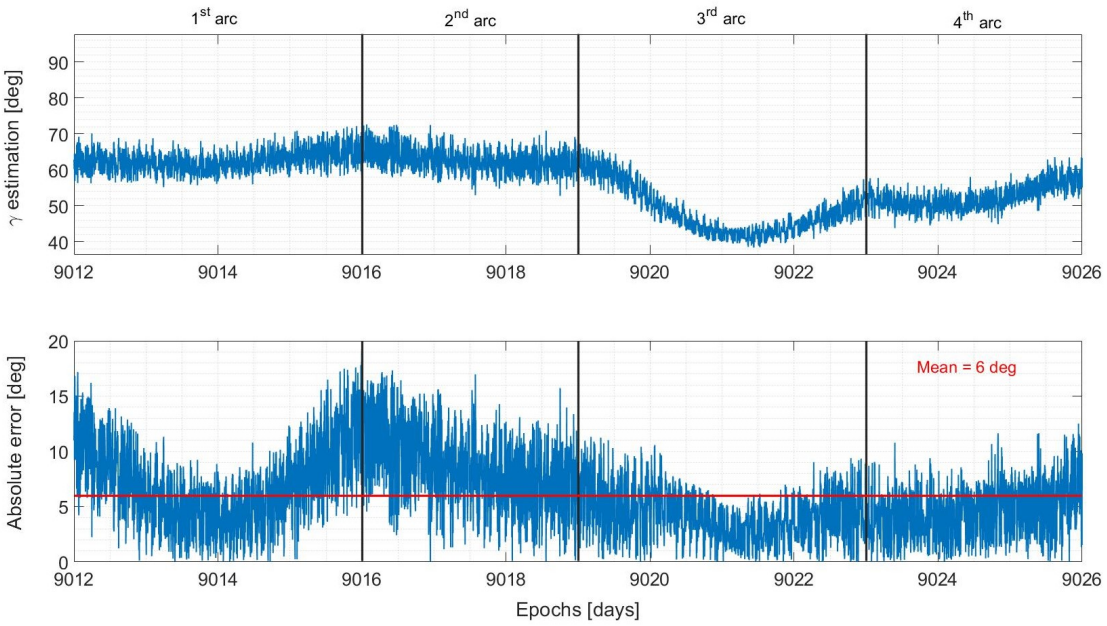

Fig. 16: Phase angle estimation

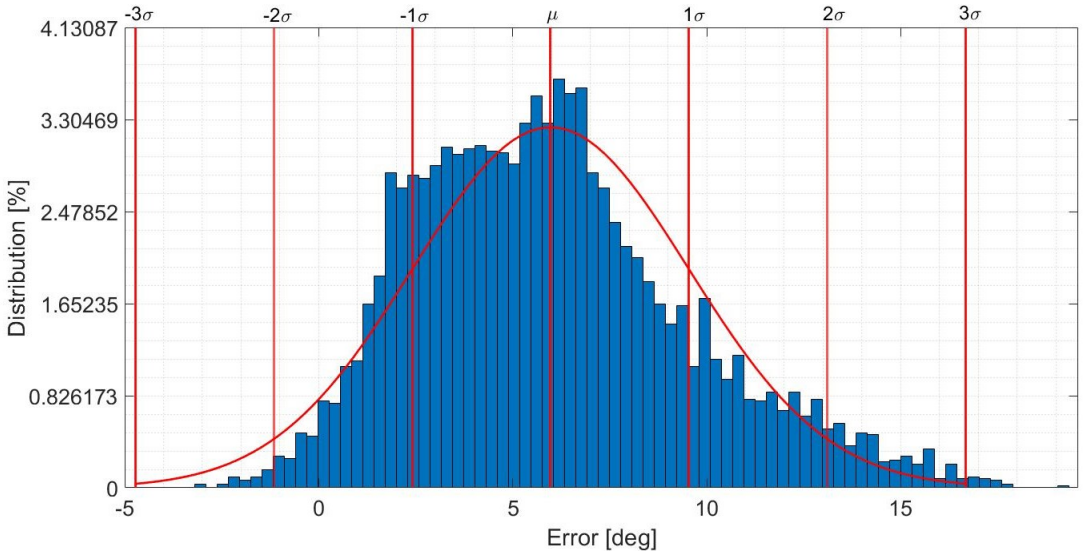

Fig. 17: Phase angle error distribution

The highest peak of the distribution is reached at 6.192° and the standard deviation is $\sigma = 3.5639°$, which means that 68.27% of the estimations have an error ranging between 9.5399°and 2.4121°. The distribution of the error is right skewed (*skewness* = 0.5654) and light-tailed (*kurtosis* = 3.0946). Ultimately, the algorithm to determine the phase angle estimation depends on a limited systematic error that is related to the approximation of the shape of the asteroid as a sphere.

5. CONCLUSIONS

This paper develops a CNN-based IP algorithm addressing the range and the phase angle estimation problem for autonomous optical navigation around a binary asteroid system. The ECP proximity operation of the Hera mission

to Didymos system is studied as case scenario. The main objective of the developed methodology is to provide the navigation algorithm with two measurements that support the position estimation of the spacecraft and the robustness of the navigation algorithm. The training, validation and testing datasets of images are generated using the software PANGU with the ECP reference trajectory. The chosen CNN architecture is the HRNet, that is the state of the art in keypoint detection and that has been already exploited for space applications. The results show that the HRNet-based IP algorithm is able to measure the pseudorange with high accuracy and the methodology is robust to the disturbances caused by the irregular shape of the asteroid and the presence of Dimorphos. In particular the percent error obtained has a near-Gaussian distribution, which is ideal for navigation filters.

The algorithm can provide an accurate estimation of the position of the SS point on the surface of the asteroid, which is used to estimate the Sun phase angle with high accuracy. Nevertheless, the methodology is influenced by systematic errors introduced by the irregular shape of the asteroid and the error does not present a Gaussian distribution. With our algorithm, we support the SSA by increasing the robustness of the navigation strategy of the first mission ever testing asteroid deflection. The unique contribution represented by the estimation of the SS point can be applied to any object in space. The pseudorange and Sun phase angle estimation methodologies can be employed for any space object with a near-spherical shape, hence it can alsoo support the tracking of space debris and other uncooperative objects.

ACKNOWLEDGMENTS

This study is co-funded and supported by the European Space Agency under the Open Space Innovation Platform and supported by GMV Defence and Space. The authors would like to thank Florin-Adrian Stancu for providing the model of Didymos in PANGU. The authors would also like to acknowledge the support of the entire Aerospace Centre of Excellence of University of Strathclyde.

6. REFERENCES

[1] N. G. Dias, P. Gordo, H. Onderwater, R. Melicio, and A. Amorim. Analysis on the Isostatic Bipod Mounts for the HERA Mission LIDAR. *Applied Sciences (Switzerland)*, 12(7), 2022.

[2] Dundee University. *Planet and Asteroid Natural Scene Generation Utility User Manual*, 2019.

[3] ESA. Hera mission instruments, 2021.

[4] ESA Esac. *HERA mission requirements document*, 2021.

[5] ESA Estec. *HERA: Proximity Operations Guidelines*, 2020.

[6] ESA Headquarters. *HERA Didymos reference model*, 2021.

[7] R. Hartley and A. Zisserman. Camera Models. *Physically Based Rendering*, pages 153–177, 2004.

[8] P. Michel, I. Carnelli, and M. Küppers. The Hera mission: European component of the ESA-NASA AIDA mission to a binary asteroid. In *COSPAR Scientific Assembly*. 2018.

[9] P. Michel, A. Cheng, and M. Küppers. Asteroid Impact and Deflection Assessment (AIDA) mission: science investigation of a binary system and mitigation test. In *European Planetary Science Congress*, pages 123–124, Nantes, France. October, 2015.

[10] NASA. JPL Solar System Dynamics, 2021.

[11] A. Pellacani, M. Graziano, M. Fittock, J. Gíl-Fernández, and I. Carnelli. HERA vision based GNC and autonomy. In *European Conference for AeroSpace Sciences*, pages 1–14, 2019.

[12] M. Pugliatti, V. Franzese, A. Rizza, F. Piccolo, C. Bottiglieri, C. Giordano, F. Ferrari, and F. Topputo. Design of the on-board image processing of the milani mission. pages 1–21, 2022.

[13] M. Pugliatti, V. Franzese, and F. Topputo. Data-Driven Image Processing for Onboard Optical Navigation Around a Binary Asteroid. *Journal of Spacecraft and Rockets*, 59(3):943–959, 2022.

[14] H. Sierks, H. U. Keller, R. Jaumann, H. Michalik, T. Behnke, F. Bubenhagen, I. Büttner, U. Carsenty, U. Christensen, R. Enge, B. Fiethe, P. Gutiérrez Marqués, H. Hartwig, H. Krüger, W. Kühne, T. Maue, S. Mottola, A. Nathues, K. U. Reiche, M. L. Richards, T. Roatsch, S. E. Schröder, I. Szemerey, and M. Tschentscher. *The Dawn framing camera*, volume 163. 2011.

[15] P. Sturm. *Pan-Tilt-Zoom (PTZ) Camera*. 2021.

[16] K. Sun, B. Xiao, L. Dong, and J. Wang. Deep high-resolution representation learning for human pose estimation. In *Proceedings of the IEEE Computer Society Conference on Computer Vision and Pattern Recognition*, pages 5686–5696. June, 2019.